Microscopic cluster model in harmonic oscillator traps

Hantao Zhang,[1,*] Dong Bai,[2,†] Zhen Wang,[1,‡] and Zhongzhou Ren[1,3,§]
[1]*School of Physics Science and Engineering, Tongji University, Shanghai 200092, China*
[2]*College of Mechanics and Engineering Science, Hohai University, Nanjing 211100, Jiangsu, China*
[3]*Key Laboratory of Advanced Micro-Structure Materials, Ministry of Education, Shanghai 200092, China*

(Received 7 November 2023; revised 28 December 2023; accepted 8 February 2024; published 12 March 2024)

Microscopic cluster model (MCM) is a successful theoretical framework to investigate nuclear clustering phenomena. In this work, we put it in a harmonic oscillator trap (HOT) and propose a new method abbreviated as MCM-HOT to study scattering states of cluster systems in free space. As proofs of concept, we compute the scattering phase shifts for some single-channel two-cluster systems. The numerical results given by MCM-HOT agree well with those from the conventional microscopic R-matrix method, implying that our novel method MCM-HOT can be useful in studying scattering processes of light neutron-nucleus systems.

DOI: 10.1103/PhysRevC.109.034307

I. INTRODUCTION

Cluster structures play an important role in nuclear many-body systems, attracting intensive attention from both experimentalists and theorists. Microscopic cluster models (MCMs) have achieved notable success in describing cluster structures by taking nucleons as building blocks and presuming the appearance of nuclear clusters. Several realizations of MCMs have been proposed in the literature, including resonating group method (RGM) [1–5], generator coordinate method (GCM) [6–8], and the Tohsaki-Horiuchi-Schuck-Röpke (THSR) wave function method [9–11]. They all follow the general philosophy of MCMs and are different from each other in technical aspects.

Due to the essential requirement for introducing open quantum systems in many-body problems, the continuous spectrum is also of paramount significance apart from the discrete bound and resonant states. Within this context, scattering phase shifts play a pivotal role as they provide fundamental insights into the interaction between nucleons, which is critical for understanding the cluster structure, studying nuclear interactions, and predicting complicated reactions. Both precise experimental measurements and theoretical calculations of scattering phase shifts are of great importance. Therefore, achieving a treatment of continuum scattering states within the MCM emerges as a crucial endeavor. Various methodologies, such as complex scaling method [12–16], microscopic R-matrix method [17–20], continuum level density method [21–24], and so on, have already been proposed to address the scattering problems.

In general, dealing with the many-body scattering problems is a more complicated task than solving bound states. If the properties of scattering states can be conveniently extracted from bound state calculations, it would facilitate a more effective approach for investigating continuum scattering states. The trap method is such an approach that involves confining particles within an artificial potential trap to extract properties of the original system. It has been successfully applied in atomic physics and nuclear physics. Explicitly speaking, the properties of elastic scattering between two particles in an infinite-volume system can be related to discrete energy spectrum of a trapped system through a closed-form formula, for example, the Busch-Englert-Rzażewski-Wilkens (BERW) formula [25] in harmonic oscillator traps [26–30]. Subsequently, the BERW formula is extended to both coupled-channel and few-body cases [31–35].

In this work, we aim to combine the trap method with the microscopic cluster model and present a comprehensive theoretical framework called MCM-HOT to calculate the scattering phase shifts, which is applicable to various implementations of microscopic cluster model such as RGM, GCM, THSR, and so on. To confirm the validation of the MCM-HOT, we take $\alpha + n$ and $\alpha + \alpha$ (without Coulomb force) systems as illustrative examples, while employing the microscopic R-matrix method as a benchmark. In addition, we introduce the complex virial theorem within the framework of MCM to ensure the accuracy of discrete energy spectrum in harmonic traps.

The rest parts are organized as follows. In Sec. II, we provide the general framework of MCM-HOT, which is applicable to different concrete MCMs such as RGM, GCM, and THSR. In Sec. III, the numerical results are presented and discussed. Section IV summarizes the article. The complex virial theorem in MCM and some formulas in GCM and THSR are included in the Appendixes.

*zhang_hantao@foxmail.com
†dbai@hhu.edu.cn
‡wang_zhen@tongji.edu.cn
§Corresponding author: zren@tongji.edu.cn

II. THEORETICAL FORMALISM

A. Microscopic cluster model

In this part, we provide a concise theoretical framework of the MCM. For more specific theoretical details of RGM, GCM, and THSR, please refer to Refs. [36,37].

Considering a system composed of A nucleons, we assume that it can be divided into two clusters with nucleon numbers A_1 and A_2. The relative coordinate $\boldsymbol{\rho}$ between two clusters and the translation-invariant internal coordinates $\boldsymbol{\xi}_{1,i}$, $\boldsymbol{\xi}_{2,j}$ can be expressed as follows:

$$\begin{aligned}\boldsymbol{\rho} &= \boldsymbol{R}_{\text{c.m.},1} - \boldsymbol{R}_{\text{c.m.},2},\\ \boldsymbol{\xi}_{1,i} &= \boldsymbol{r}_i - \boldsymbol{R}_{\text{c.m.},1},\ i = 1,\ldots,A_1,\\ \boldsymbol{\xi}_{2,j} &= \boldsymbol{r}_j - \boldsymbol{R}_{\text{c.m.},2},\ j = A_1+1,\ldots,A_1+A_2,\end{aligned} \tag{1}$$

where $\boldsymbol{R}_{\text{c.m.},1}$ and $\boldsymbol{R}_{\text{c.m.},2}$ are the center-of-mass (c.m.) coordinates of two clusters.

In the RGM, the total wave function can be constructed from the internal cluster wave functions (denoted as ϕ_1 and ϕ_2 for two-cluster system). These internal wave functions are obtained through a harmonic oscillator model with an oscillator parameter represented as b. Generally, it is assumed that the oscillator parameters of all clusters are the same. Deviating from this assumption can lead to serious technical challenges due to spurious c.m. components. For two-cluster systems, the RGM wave function can be formulated as

$$\begin{aligned}\Psi(\xi_{1,i},\xi_{2,j},\boldsymbol{\rho}) &= \mathscr{A}\phi_1(\xi_{1,i})\phi_2(\xi_{2,j})g(\boldsymbol{\rho})\\ &= \int \mathscr{A}\phi_1(\xi_{1,i})\phi_2(\xi_{2,j})\delta(\boldsymbol{\rho}-\boldsymbol{r})g(\boldsymbol{r})d\boldsymbol{r},\end{aligned} \tag{2}$$

where $g(\boldsymbol{\rho})$ is the relative wave function and needs to be determined by solving the Schrödinger equation. $\mathscr{A}$ represents the antisymmetrization operator.

After substituting this wave function into the Schrödinger equation, we obtain the RGM equation

$$\int (\mathscr{H}(\boldsymbol{\rho},\boldsymbol{\rho}') - E_{\text{total}}\mathscr{N}(\boldsymbol{\rho},\boldsymbol{\rho}'))g(\boldsymbol{\rho}')d\boldsymbol{\rho}' = 0, \tag{3}$$

where $\mathscr{H}$ and $\mathscr{N}$ are the nonlocal overlap and Hamiltonian kernels defined as

$$\begin{Bmatrix}\mathscr{H}(\boldsymbol{\rho},\boldsymbol{\rho}')\\ \mathscr{N}(\boldsymbol{\rho},\boldsymbol{\rho}')\end{Bmatrix} = \langle\phi_1\phi_2\delta(\boldsymbol{\rho}-\boldsymbol{r})|\begin{Bmatrix}H\\ 1\end{Bmatrix}|\mathscr{A}\phi_1\phi_2\delta(\boldsymbol{\rho}'-\boldsymbol{r})\rangle\,, \tag{4}$$

where the integrals are performed over the internal coordinates $\boldsymbol{\xi}$ and the relative coordinate $\boldsymbol{r}$. The kinetic energy of the c.m. has already been subtracted in the Hamiltonian H.

In the GCM framework, the Brink wave function of two-cluster can be expressed through the Slater determinant

$$\begin{aligned}\Phi(\boldsymbol{R}) &= \frac{1}{\sqrt{A!}}\det\left\{\hat{\phi}_1\left(-\frac{A_2}{A}\boldsymbol{R}\right)\cdots\hat{\phi}_{A_1}\left(-\frac{A_2}{A}\boldsymbol{R}\right)\right.\\ &\left.\times\,\hat{\phi}_{A_1+1}\left(\frac{A_1}{A}\boldsymbol{R}\right)\cdots\hat{\phi}_A\left(\frac{A_1}{A}\boldsymbol{R}\right)\right\}\\ &= \sqrt{\frac{A_1!A_2!}{A!}}\mathscr{A}\left[\Phi_1\left(-\frac{A_2}{A}\boldsymbol{R}\right)\Phi_2\left(\frac{A_1}{A}\boldsymbol{R}\right)\right],\end{aligned} \tag{5}$$

the individual orbitals $\hat{\phi}$ are factorized in space, spin, and isospin components:

$$\hat{\phi}(\boldsymbol{S}) = \phi(\boldsymbol{r},\boldsymbol{S})\chi_{\sigma\tau}, \tag{6}$$

where $\chi_{\sigma\tau}$ is the spin-isospin wave function. The radial part $\phi(\boldsymbol{r},\boldsymbol{S})$ is an harmonic oscillator function. In the case of s wave, it reads

$$\phi_{0s}(\boldsymbol{r},\boldsymbol{S}) = (\pi b^2)^{-3/4}\exp\left(-\frac{(\boldsymbol{r}-\boldsymbol{S})^2}{2b^2}\right), \tag{7}$$

where b is called the oscillator parameter. When assuming a common oscillator parameter b, Eq. (5) can be rewritten as

$$\Phi(\boldsymbol{R}) = \sqrt{\frac{A_1!A_2!}{A!}}\Phi_{\text{c.m.}}\mathscr{A}[\phi(c_1)\phi(c_2)\Gamma(\boldsymbol{\rho},\boldsymbol{R})], \tag{8}$$

which involves the translation-invariant functions $\phi(c_1)$ and $\phi(c_2)$ of two clusters. The center of mass and radial wave functions read

$$\Phi_{\text{c.m.}}(\boldsymbol{R}_{\text{c.m.}}) = \left(\frac{A}{\pi b^2}\right)^{3/4}\exp\left(-\frac{A}{2b^2}\boldsymbol{R}_{\text{c.m.}}^2\right), \tag{9}$$

$$\Gamma(\boldsymbol{\rho},\boldsymbol{R}) = \left(\frac{\mu_0}{\pi b^2}\right)^{3/4}\exp\left(-\frac{\mu_0}{2b^2}(\boldsymbol{\rho}-\boldsymbol{R})^2\right), \tag{10}$$

where μ_0 equals $\frac{A_1A_2}{A_1+A_2}$.

The overlap kernel $N(\boldsymbol{R},\boldsymbol{R}')$ and Hamiltonian kernel $H(\boldsymbol{R},\boldsymbol{R}')$ are calculated by

$$\begin{aligned}N(\boldsymbol{R},\boldsymbol{R}') &= \langle\Phi(\boldsymbol{R})|\,|\Phi(\boldsymbol{R}')\rangle\,,\\ H(\boldsymbol{R},\boldsymbol{R}') &= \langle\Phi(\boldsymbol{R})|\,H\,|\Phi(\boldsymbol{R}')\rangle\,.\end{aligned} \tag{11}$$

In contrast to the traditional picture of localized clustering (Brink wave function in the GCM), nuclear clusters in the nonlocalized cluster model are not fixed to specific geometric positions but can move freely in a hypothetic nuclear container. For $n\alpha$ boson system, the nonlocalized THSR wave function can be expressed as a superposition of localized Brink wave functions $\Phi^B(\boldsymbol{R}_1,\ldots,\boldsymbol{R}_n)$:

$$\begin{aligned}\Phi_{n\alpha}(\beta_x,\beta_y,\beta_z) &= \int d^3R_1\cdots d^3R_n\exp\left\{-\sum_{i=1}^{n}\left(\frac{R_{ix}^2}{\beta_x^2}+\frac{R_{iy}^2}{\beta_y^2}+\frac{R_{iz}^2}{\beta_z^2}\right)\right\}\Phi^B(\boldsymbol{R}_1,\cdots,\boldsymbol{R}_n),\\ \Phi^B(\boldsymbol{R}_1,\cdots,\boldsymbol{R}_n) &= \det\{\phi_{0s}(\boldsymbol{r}_1,\boldsymbol{R}_1)\chi_{\sigma_1\tau_1}\cdots\phi_{0s}(\boldsymbol{r}_{4n},\boldsymbol{R}_n)\chi_{\sigma_{4n}\tau_{4n}}\},\end{aligned} \tag{12}$$

where β_x, β_y, β_z represent the deformation parameters along three directions. For two α system we only handle the case of axially symmetric deformation with the z axis being the symmetry axis, namely, $\beta_x = \beta_y \neq \beta_z$.

The harmonic oscillator potential between two clusters can be introduced by adding a direct local potential $\frac{1}{2}\mu\omega^2 r^2$ in RGM equation. As for GCM and THSR, introducing the harmonic oscillator potential can be achieved through the corresponding asymptotic relative wave functions. Specific details can be found in Appendix B. For n clusters in the MCM, the introduction of harmonic oscillator traps follows a similar procedure. In the RGM, this means that for each of the $n-1$ coordinates within each Jacobi coordinate, we introduce a local harmonic oscillator potential with the relevant reduced mass. In the case of GCM and THSR, $n-1$ asymptotic relative wave functions within each Jacobi coordinate should be utilized to construct the matrix elements.

B. Harmonic oscillator trap

Generally, the scattering phase shift of two particles can be formulated by the discrete energy spectrum of the trapped system in a closed form:

$$\det[\cot(\delta(E)) - \mathscr{F}^{\text{trap}}(E)] = 0, \tag{13}$$

where $\delta(E)$ represents the diagonal matrix of scattering phase shifts, and the analytic matrix function $\mathscr{F}^{\text{trap}}(E)$ is determined through the geometric and dynamic properties of the trap itself, which can be derived through the quantization condition.

If considering a harmonic oscillator potential, a formula about the scattering length term for two cold atoms trapped in it is initially proposed in Ref. [25], and later, it is extended to compute full energy-dependent phase shifts and applied to cases for partial waves beyond s wave. Here, it is called Busch-Englert-Rzażewski-Wilkens (BERW) and formulated for angular momentum l as

$$\cot(\delta_l(E)) = (-1)^{l+1}\left(\frac{4\mu\omega}{k^2}\right)^{l+1/2}\frac{\Gamma\left(\frac{3}{4}+\frac{l}{2}-\frac{E}{2\omega}\right)}{\Gamma\left(\frac{1}{4}-\frac{l}{2}-\frac{E}{2\omega}\right)}, \tag{14}$$

where μ is the reduced mass and δ_l is the scattering phase shift. This formula holds at the eigenenergies $E = \frac{k^2}{2\mu}$ with the center-of-mass energy already subtracted. In a harmonic trap each particle experiences a potential $\frac{1}{2}M\omega^2 r^2$, where M is its mass. One can only deal with the relative motion of two particles based on the fact that the center-of-mass motion can be factorized, namely, the interaction caused by harmonic oscillator trap can be directly written as $\frac{1}{2}\mu\omega^2 r^2$, where r is the relative coordinate.

For a two-body system with short-range interactions, the analytic matrix function $\mathscr{F}^{\text{trap}}(E)$ in Eq. (13) can be formulated in a generalized form [32]

$$\mathscr{F}_l^{\text{trap}}(E) = \frac{2^{2l+2}\Gamma(l+3/2)^2}{2\mu k^{2l+1}\pi}\left(\frac{\Re\left[G_l^{\text{free}}(r,r',k)\right]}{(rr')^l}\Big|_{r,r'\to 0} - \frac{G_l^{\text{trap}}(r,r',E)}{(rr')^l}\Big|_{r,r'\to 0}\right), \tag{15}$$

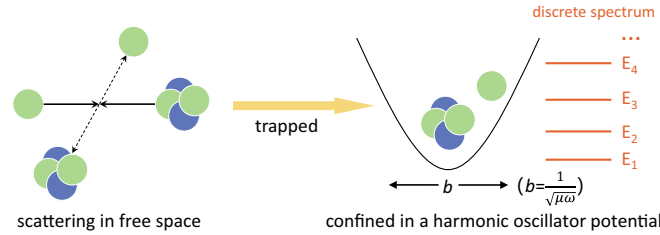

FIG. 1. Left: scattering of α particle and neutron in free space. Right: by introducing an artificial potential trap (illustrated here with harmonic oscillator trap), α particle and neutron are confined in it. The scattering properties in an infinite volume on the left can be linked to the discrete energy spectra inside the trap on the right. The trap size b is required to be much larger than the range of short-range interactions between particles.

where $G_l^{\text{free}}(r,r',k)$ is the free particle Green's function

$$G_l^{\text{free}}(r,r',k) = -2i\mu k j_l(kr_<)h_l^{(+)}(kr_>), \tag{16}$$

where j_l and $h_l^{(+)}$ are regular spherical Bessel and Hankel functions with $k = \sqrt{2\mu E}$ being the wave number, $r_<$ and $r_>$ denote the lesser and greater of (r,r'), respectively. For the harmonic oscillator trap, the trap Green's function $G_l^{\text{trap}}(r,r',E)$ can be written as $G_l^{\omega}(r,r',E)$ [38],

$$G_l^{\omega}(r,r',E) = -\frac{1}{\omega(rr')^{3/2}}\frac{\Gamma\left(\frac{l}{2}+\frac{3}{4}-\frac{E}{2\omega}\right)}{\Gamma\left(l+\frac{3}{2}\right)} \times \mathscr{M}_{\frac{E}{2\omega},\frac{l}{2}+\frac{1}{4}}(\mu\omega r_<^2)\mathscr{W}_{\frac{E}{2\omega},\frac{l}{2}+\frac{1}{4}}(\mu\omega r_>^2), \tag{17}$$

where $\mathscr{M}_{a,b}(z)$ and $\mathscr{W}_{a,b}(z)$ are the Whittaker functions [39], $r_<$ and $r_>$ denote the lesser and greater of (r,r'), respectively.

The BERW formula can be easily obtained through Eqs. (13) and (15). For other types of traps such as spherical hard wall trap [40–42], periodic cubic box, and so on, obtaining their corresponding Green's functions is sufficient. Afterwards, following the framework outlined above, closed-form phase shift formulas for these traps can be derived. More detailed derivations can be found in Ref. [43].

The original BERW formula [Eq. (14)] is derived under the assumption of short-range interactions, without taking into account the long-range interactions. In the presence of the Coulomb potential, Eq. (14) is not applicable and requires complicated Coulomb corrections. At low energy, the long-range Coulomb potential plays an important role for charged particles. However, only in a few cases can the Coulomb potential be analytically incorporated within trap method, such as spherical hard wall and the confining potential described in [44], where the potential equals 0 within a certain radius and tends toward infinity as distance approaches infinity. Investigating the microscopic cluster model within these potentials may be also interesting.

By adding an artificial trap the particles are confined in a finite volume and only bound states exist (as shown in Fig. 1). The properties of scattering in infinite free space is encoded in the confined system and connected with the eigenstates in the trap through quantization condition. Furthermore, in order to construct an interaction-independent modeling, the size of

the finite volume induced by the trap should be significantly larger than the range of short-range interactions, namely, the width of the trap, denoted as b, should be guaranteed to satisfy $b \gg R_{\text{inter}}$, where R_{inter} is the interaction range between particles. Therefore, we can find a region within the trap where the interactions are insignificant. In this case, a connection between the asymptotic form of the scattering wave function with the trapped wave function can be established. Specifically for the harmonic oscillator trap, two spatial scales need to satisfy $b_\omega = \frac{1}{\sqrt{\mu\omega}} \gg R_{\text{inter}}$.

III. NUMERICAL RESULTS

We have already implemented the harmonic oscillator trap into the MCM with a generalized approach. In the following part, we take $\alpha + n$ system handled with RGM as a proof-of-concept example. As mentioned in the previous section, the harmonic oscillator trap is introduced by adding a local interaction $\frac{1}{2}\mu\omega^2 r^2$, which leads to the following new RGM equation:

$$\begin{aligned}&\left\{\frac{1}{2\mu}\left[\frac{d^2}{dr^2} - \frac{l(l+1)}{r^2}\right] + E - V_N(r) - \eta_{Jl}V_{s.o.}(r)\right.\\&\left. - \frac{1}{2}\mu\omega^2 r^2\right\}\phi_{Jl}(r)\\&= \int_0^\infty \left[k_l^N(r,r') + k_l^C(r,r') + \eta_{Jl}k_l^{s.o.}(r,r')\right]\phi_{Jl}(r')dr'\end{aligned} \tag{18}$$

with

$$\eta_{Jl} = \begin{cases} l, & J = l + 1/2 \\ -(l+1), & J = l - 1/2 \end{cases}, \tag{19}$$

where direct nuclear potential V_N and direct spin-orbit potential $V_{s.o.}$, exchange potentials k_l^N, k_l^C, and $k_l^{s.o.}$ can be found in Refs. [45–47].

The oscillator parameter b is set to 1.395 fm for $\alpha + n$, and the parameters in nucleon-nucleon potentials are all chosen from Ref. [46]. In addition, it should be noted that the parameters for the spin-orbit interaction we utilized correspond to the set I as defined in Ref. [46].

For a given parameter ω, solving the new RGM equation above yields a discrete energy spectrum. With the BERW formula, the corresponding phase shifts at these eigenenergies (excluding negative eigenenergies) can be obtained. In practice, the choice of ω should strike a balance between achieving precision in bound-state solutions (i.e., ω should not be too small) and satisfying the constraint imposed by the trap method itself, which requires that ω should not be too large. In other words, the width $b_\omega = \frac{1}{\sqrt{\mu\omega}}$ of the harmonic oscillator potential trap should be larger than the range of cluster-cluster short-range interactions as much as possible. The specific range of ω will be provided in the subsequent calculations and discussions.

In solving the RGM equation, we employ the Gaussian basis functions $\phi_{nl}^G(r) = N_{nl} r^l e^{-r^2/r_n^2}$ to expand the wave function, with parameters $r_i = r_0\gamma^{i-1}$, $i = 1, 2, \ldots, 30$, where $r_0 = 0.1$ fm and $\gamma = 1.2$. We begin our discussion by considering the case of $l = 0$. Figure 2 illustrates the s-wave scattering phase shifts for $\alpha + n$. The solid line represents results obtained using the traditional microscopic R-matrix method (for more specific details, please refer to Refs. [18,48]), while the circular, triangular, and square markers correspond to results obtained through the MCM-HOT using the first, second, and third eigenenergies, respectively. Here, we have set the maximum value of ω to be 1.5 MeV, and all eigenvalue calculations have undergone verification through the virial theorem to reduce errors stemming from BERW's sensitivity to input energies. As mentioned above, due to the inherent constraints of the trap method, ω cannot be excessively large, as it would result in an overly narrow harmonic oscillator trap. In our calculations, we have also observed that taking an excessively large value for ω will lead to inaccuracies in the results of phase shifts.

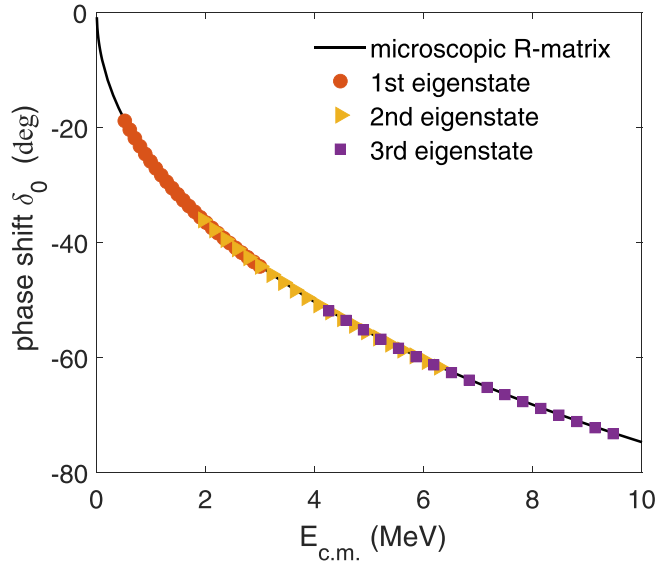

FIG. 2. The phase shifts of s-wave $\frac{1}{2}^+$ state computed with microscopic R matrix and MCM-HOT. The solid line represents results with microscopic R-matrix method, the circular, triangular, and square markers correspond to results obtained with MCM-HOT using the first, second, and third eigenenergies, respectively. For these first three eigenstates, the maximum values of ω adopted are all less than or equal to 1.5 MeV. For the first, second, and third eigenstates, the values of ω are $\{0.30, 0.35, 0.40, \ldots, 1.50\}$ MeV, $\{0.50, 0.55, 0.60, \ldots, 1.50\}$ MeV, and $\{0.70, 0.75, 0.80, \ldots, 1.50\}$ MeV, respectively.

For the s-wave case, we observe a very good consistency between the results obtained through MCM-HOT and the traditional microscopic R-matrix method. Next, we will examine two states $\frac{1}{2}^-$ and $\frac{3}{2}^-$ corresponding to the p wave to further validate the reliability of our approach.

Figure 3(a) and 3(b) displays the scattering phase shifts for $\frac{1}{2}^-$ and $\frac{3}{2}^-$ states, respectively. The solid lines still represent results obtained using the microscopic R-matrix method. In MCM-HOT, we utilize the first four eigenstates, indicated by circular, square, triangular, and rhombus markers, to compute the scattering phase shifts. The maximum value of ω is still taken to be 1.5 MeV as the same as the s-wave case. It is

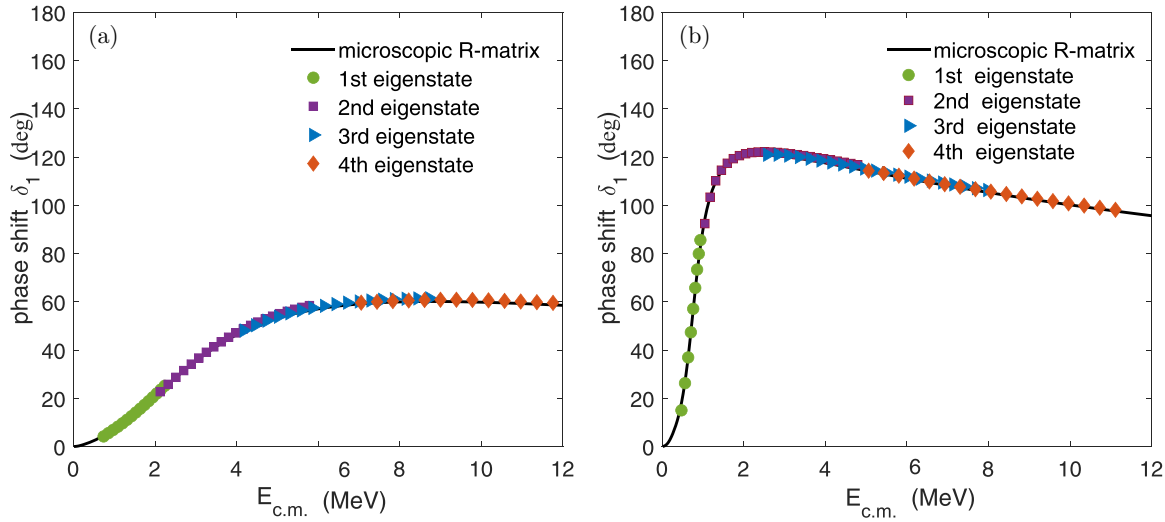

FIG. 3. (a) The phase shifts of $\frac{1}{2}^-$ state computed with microscopic R matrix and MCM-HOT. For the first, second, third and fourth eigenstates, the values of ω are $\{0.30, 0.35, 0.40, \ldots, 1.00\}$ MeV, $\{0.50, 0.55, 0.60, \ldots, 1.50\}$ MeV, $\{0.70, 0.75, 0.80, \ldots, 1.50\}$ MeV, and $\{0.90, 0.95, 1.00, \ldots, 1.50\}$ MeV, respectively. (b) The phase shifts of $\frac{3}{2}^-$ state computed with microscopic R matrix and MCM-HOT. The maximum values of ω are also all less than or equal to 1.5 MeV for first four eigenstates. In both (a) and (b), the circular, square, triangular, and rhombus markers correspond to the results calculated with MCM-HOT using the first, second, third, and fourth eigenenergies, respectively, the solid lines represent results with microscopic R matrix. For the first, second, third, and fourth eigenstates, the values of ω are $\{0.20, 0.25, 0.30, \ldots, 0.60\}$ MeV, $\{0.30, 0.35, 0.40, \ldots, 1.50\}$ MeV, $\{0.50, 0.55, 0.60, \ldots, 1.50\}$ MeV, and $\{0.70, 0.75, 0.80, \ldots, 1.50\}$ MeV, respectively.

evident that MCM-HOT performs well for these two resonant states corresponding to the p wave. Moreover, MCM-HOT can accurately reproduce the rapidly varying portions of the phase shift curves at lower energies, which also indicates that MCM-HOT offers a high accuracy.

As another supplement, we apply the MCM-HOT to the α-α system (without Coulomb potential) within GCM and THSR frameworks. As previously mentioned, the harmonic oscillator trap is introduced into GCM and THSR via asymptotic relative wave functions. The parameters used in the calculation can also be found in the Appendix B.

Figures 4 and 5 demonstrate the scattering phase shifts calculated by microscopic R-matrix method and MCM-HOT in GCM and THSR frameworks, respectively. The three subfigures in each figure correspond to the results of S, D, and G waves, respectively. We mark the results from R-matrix method with solid lines, the square, circle, left-triangle, right-triangle symbols represent the phase shifts extracted from different eigenstates of trapped system. It should be noted that for both D and G waves we have chosen the energies of the first four eigenstates. However, since the first eigenenergy of S wave may be negative, which should be eliminated, we have utilized the second to the fifth eigenstates for the S wave. In addition, we have chosen the same upper limit of 1.5 MeV for ω, while the lower limit is determined through the virial theorem. In other words, we exclude values of ω that are too small and would result in insufficient accuracy in bound-state solutions.

We can find that regardless of GCM and THSR, the numerical results obtained by MCM-HOT for scattering phase shifts are consistent very well with each other, as well as being in pretty good agreement with the results from R-matrix method. This further validates the reliability of employing different cluster methods within the MCM-HOT framework. As for hybrid models like Brink-THSR, a similar approach can also be applied to introduce the harmonic oscillator trap, with the only distinction being the more complicated asymptotic relative wave function. Furthermore, MCM-HOT employed here can also conveniently be implemented into general few-cluster GCM or THSR frameworks.

As an additional supplement for accuracy of bound state solutions, in Figs. 6 and 7, we illustrate the verification with the virial theorem using the $\frac{1}{2}^-$ state of $\alpha + n$ system and the 2^+ state of $\alpha + \alpha$ system (without Coulomb potential) as examples. The figures display the phase shifts obtained from MCM-HOT, the eigenenergies and their deviation from the virial theorem. When the eigenenergy and the wave function obtained within RGM framework are assumed as the "exact" solutions $E_{\text{c.m.}}$ and ψ, we can define E_{Virial} as the energy obtained by utilizing the virial theorem mentioned in Appendix A:

$$
\begin{aligned}
E_{\text{Virial}} = \Bigg\{ \frac{1}{2} \Bigg[& \langle\psi| r \frac{\partial V(r)}{\partial r} \\
& + W(r,r') + r \frac{\partial W(r,r')}{\partial r} + r' \frac{\partial W(r,r')}{\partial r'} |\psi\rangle \\
& + E_{\text{c.m.}} \langle\psi| N(r,r') + r \frac{\partial N(r,r')}{\partial r} + r' \frac{\partial N(r,r')}{\partial r'} |\psi\rangle \Bigg] \\
& + V(r) + W(r,r') \Bigg\} / \langle\psi| 1 - N(r,r') |\psi\rangle \,, \qquad (20)
\end{aligned}
$$

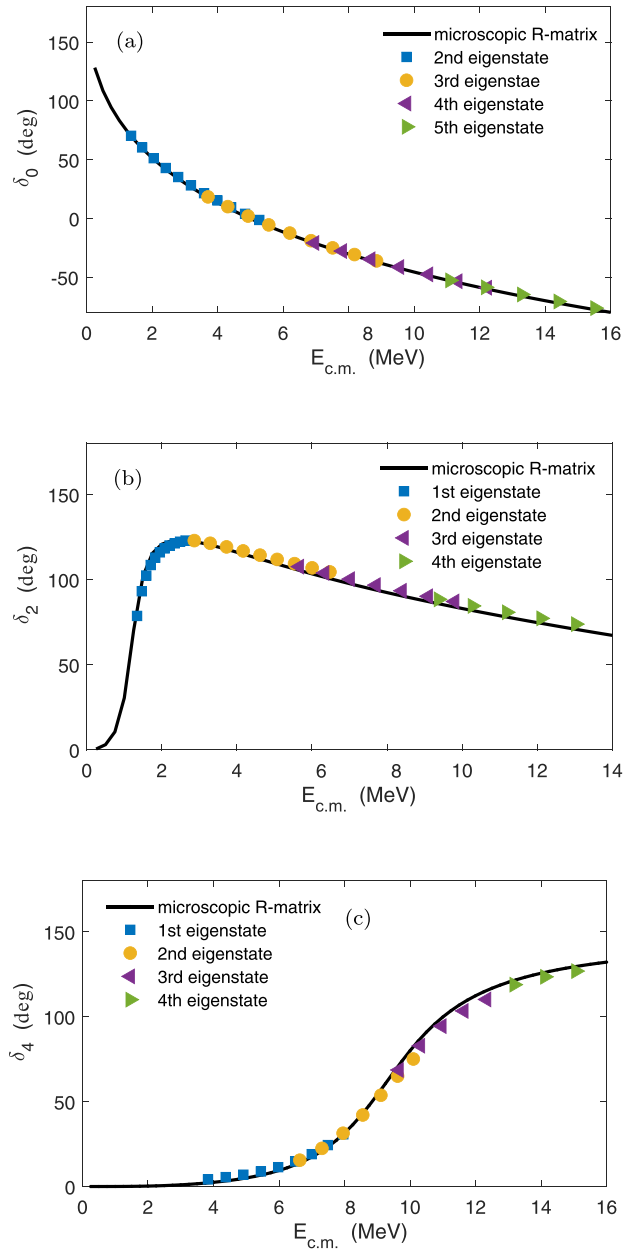

FIG. 4. (a), (b), (c) The phase shifts of 0^+, 2^+ and 4^+ states of $\alpha + \alpha$ system (without Coulomb interaction) computed with microscopic R matrix and MCM-HOT in the GCM framework. For the eigenstates utilized, the maximum values of ω adopted are all less than or equal to 1.5 MeV. For 0^+ state, $\omega_{\min}$ corresponding to the second, third, fourth, and fifth eigenstates are 0.50, 0.70, 0.90, 1.10 MeV, respectively. For 2^+ state, $\omega_{\min}$ corresponding to the first, second, third, and fourth eigenstates are 0.50,0.70,0.90,1.10 MeV, respectively. For 4^+ state, $\omega_{\min}$ corresponding to the first, second, third, and fourth eigenstates are 0.70, 0.90, 1.10, 1.30 MeV, respectively. The step size for ω is 0.10 MeV. The 21 generator coordinates used for solving the bound states are uniformly distributed in the range [0.1, 21] fm.

FIG. 5. (a), (b), (c) The phase shifts of 0^+, 2^+, and 4^+ states of $\alpha + \alpha$ system (without Coulomb interaction) computed with microscopic R matrix and MCM-HOT in THSR framework. For the eigenstates utilized, the maximum values of ω adopted are all less than or equal to 1.5 MeV. For 0^+ state, $\omega_{\min}$ corresponding to the second, third, fourth, and fifth eigenstates are 0.50,0.70,0.90,1.10 MeV, respectively. For 2^+ state, $\omega_{\min}$ corresponding to the first, second, third, and fourth eigenstates are 0.50, 0.70, 0.90, 1.10 MeV, respectively. For the 4^+ state, $\omega_{\min}$ corresponding to the first, second, third, and fourth eigenstates are 0.80, 1.00, 1.10, 1.30 MeV, respectively. The step size for ω is 0.10 MeV. The parameters of the THSR wave functions used for solving the bound states are $\frac{\beta_\perp}{b^2} = 0.5, 1, 2, \ldots, 10$, $\beta_z = 10^{-6}$ fm.

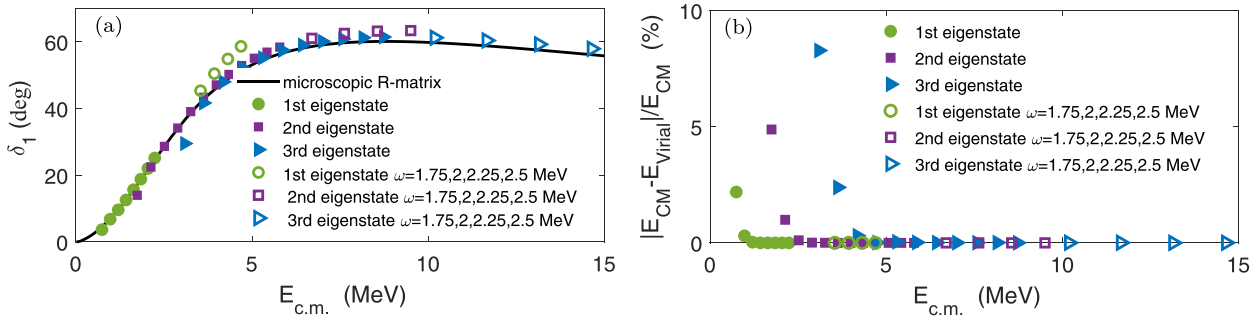

FIG. 6. (a) The phase shifts of $\frac{1}{2}^-$ state for $\alpha + n$ system obtained by MCM-HOT and R-matrix method with first three eigenstates. For the first, second, and third eigenstates, the solid symbols correspond to the following ω values: $\{0.3, 0.4, 0.5, \ldots, 1.0\}$ MeV, $\{0.4, 0.5, 0.6, \ldots, 1.5\}$ MeV, and $\{0.5, 0.6, 0.7, \ldots, 1.5\}$ MeV, respectively. The hollow symbols correspond to $\omega = \{1.75, 2, 2.25, 2.5\}$ MeV. (b) The discrepancy between E_{Virial} and the eigenenergy $E_{\text{c.m.}}$, The horizontal axis represents the numerical eigenenergy, while the vertical axis displays the percentage difference between the values of $E_{\text{c.m.}}$ and E_{Virial} relative to $E_{\text{c.m.}}$.

as for GCM and THSR frameworks, E_{Virial} can be defined as

$$E_{\text{Virial}} = \begin{cases} \left.\dfrac{\partial_\eta \sum_{i,j}(C_i\psi(\eta R_i)|H|C_j\psi(\eta R_j))}{\partial_\eta \sum_{i,j}(C_i\psi(\eta R_i)|C_j\psi(\eta R_j))}\right|_{\eta=1} & \text{GCM} \\ \left.\dfrac{\partial_\eta \sum_{i,j}(C_i\psi(\eta \boldsymbol{\beta}_i)|H|C_j\psi(\eta \boldsymbol{\beta}_j))}{\partial_\eta \sum_{i,j}(C_i\psi(\eta \boldsymbol{\beta}_i)|C_j\psi(\eta \boldsymbol{\beta}_j))}\right|_{\eta=1} & \text{THSR} \end{cases}, \tag{21}$$

where $\eta = e^{i\theta}$ is introduced by the complex scaling method. The parentheses "()" used above denote the c product required by the non-Hermitian nature induced by the complex scaling transformation.

From Figs. 6(b) and 7(b), it's apparent that when there's a significant discrepancy between E_{Virial} and the eigenenergy $E_{\text{c.m.}}$, indicating inadequate accuracy in solving the bound state, there is a considerable deviation in the phase shift obtained through MCM-HOT. Therefore, considering the necessity of the virial theorem, results with a large $|E_{\text{Virial}} - E_{\text{c.m.}}|/E_{\text{c.m.}}$ discrepancy should be disregarded. In the examples computed here, we have found that this relative deviation ideally should be less than around 1%. For other states of $\alpha + n$ and other states of $\alpha + \alpha$ (without Coulomb interaction) in the GCM framework, as well as computations in the THSR framework, the results of the virial theorem follow a similar pattern as shown in Figs. 6 and 7. Generally speaking, for the same eigenstate, the smaller the value of ω, the greater the deviation between eigenenergy and the virial theorem; for the same ω, higher energy levels exhibit larger deviations between eigenenergy and the virial theorem.

Based on condition $b_\omega = \frac{1}{\sqrt{\mu\omega}} \gg R_{\text{inter}}$, it is preferable for ω to have smaller values. However, in practical computations, considering the precision of eigenenergy solutions and the need to cover a broad range of scattering energies, is is often impractical to make b_ω significantly larger than R_{inter}. We need to strike a balance to determine an appropriate range for ω. In the examples we have calculated, setting the upper limit of ω to be less than or equal to 1.5 MeV seems reasonably suitable. In Figs. 6 and 7, we also demonstrate the phase shifts obtained from larger ω with hollow symbols, along with the discrepancy between the eigenenergy and the virial theorem. It is noticeable that as ω continues to increase, the difference between the phase shifts obtained through MCM-HOT and

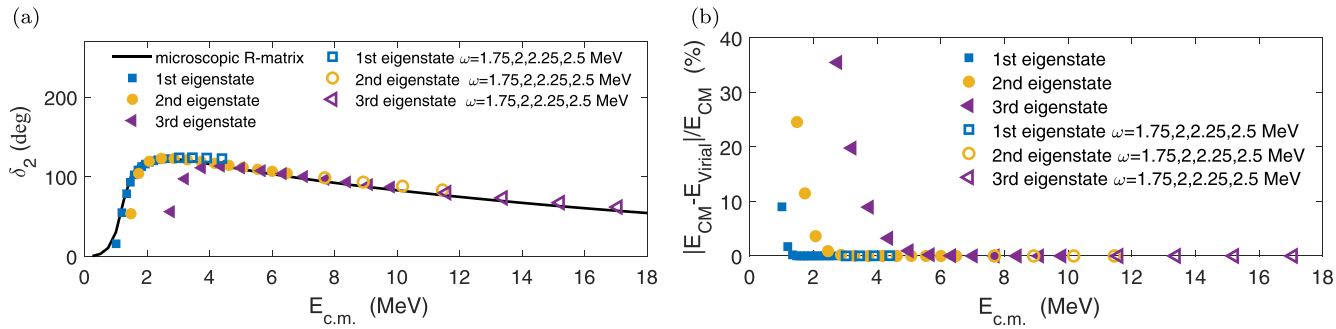

FIG. 7. (a) The phase shifts of 2^+ state for $\alpha + \alpha$ system (without Coulomb potential) obtained by MCM-HOT and R-matrix method with first three eigenstates. For the first, second, and third eigenstates, the solid symbols correspond to the following ω values: $\{0.3, 0.4, 0.5, \ldots, 1.5\}$ MeV, $\{0.3, 0.4, 0.5, \ldots, 1.5\}$ MeV, and $\{0.4, 0.5, 0.6, \ldots, 1.5\}$ MeV, respectively. The hollow symbols correspond to $\omega = \{1.75, 2, 2.25, 2.5\}$ MeV. (b) The discrepancy between E_{Virial} and the eigenenergy $E_{\text{c.m.}}$, The horizontal axis represents the numerical eigenenergy, while the vertical axis displays the percentage difference between the values of $E_{\text{c.m.}}$ and E_{Virial} relative to $E_{\text{c.m.}}$.

TABLE I. The phase shifts obtained by MCM-HOT and R-matrix method with some typical values of ω for the first three eigenvalues (for 0^+ state of $\alpha+\alpha$ (without Coulomb potential), the second, third and fourth eigenvalues). For a particular eigenstate of each state, three ω values are chosen as examples for performing computations of $\alpha+n$ system in RGM framework, and $\alpha+\alpha$ system (without Coulomb potential) in GCM and THSR frameworks. In both GCM and TSHR framework, the channel radius in R-matrix method is taken as 8 fm, and in RGM calculations the channel radius is taken as 11 fm. In the R-matrix method the parameters of the THSR wave functions are $\frac{\beta_\perp}{b^2}=0.5, 1, 1.5, 2, 2.5, 3, 4, \ldots, 11$, $\beta_z=\tan(\frac{\pi}{8})\beta_\perp$ fm and the generator coordinates used in GCM framework are $R=1, 2, \ldots, 15$ fm.

$\alpha+n$ RGM framework

	1st eigenstate				2nd eigenstate				3rd eigenstate			
state	ω(MeV)	E(MeV)	δ^{BERW} (°)	$\delta_1^{R-\mathrm{matrix}}$ (°)	ω	E	δ^{BERW}	$\delta^{R-\mathrm{matrix}}$	ω	E	δ^{BERW}	$\delta^{R-\mathrm{matrix}}$
$\frac{1}{2}^+$	0.3	0.5139	−18.85	−18.78	0.5	1.951	−36.08	−35.99	0.7	4.254	−51.89	−51.79
	0.9	1.691	−33.67	−33.61	1.0	4.066	−50.84	−50.74	1.1	6.832	−63.93	−63.82
	1.5	2.993	−44.16	−44.06	1.5	6.279	−61.66	−61.55	1.5	9.471	−73.25	−73.10
$\frac{1}{2}^-$	0.3	0.7367	4.198	4.453	0.5	2.126	22.75	22.63	0.7	4.178	48.13	47.57
	0.7	1.635	15.67	15.39	1.0	3.983	47.10	45.92	1.1	6.431	59.05	58.02
	1.0	2.236	25.16	24.28	1.5	5.785	58.43	56.28	1.5	8.729	61.47	60.15
$\frac{3}{2}^-$	0.2	0.4684	15.01	17.85	0.3	1.042	92.43	93.40	0.5	2.576	121.0	121.0
	0.4	0.7566	57.09	55.45	0.9	2.823	121.9	120.7	1.0	5.226	114.4	113.7
	0.6	0.9334	85.60	81.74	1.5	4.791	116.8	115.1	1.5	7.975	106.3	105.4

$\alpha+\alpha$ (without Coulomb) GCM framework

	2nd eigenstate				3rd eigenstate				4th eigenstate			
0^+	0.5	1.359	70.28	70.05	0.7	3.707	18.31	17.89	0.9	6.959	−20.88	−21.09
	1.0	3.186	28.08	26.61	1.1	6.203	−12.48	−13.67	1.2	9.552	−41.36	−42.42
	1.5	5.272	−1.317	−3.399	1.5	8.853	−36.13	−37.17	1.5	12.23	−58.95	−60.07
	1st eigenstate				2nd eigenstate				3rd eigenstate			
2^+	0.5	1.340	78.63	84.41	0.7	2.865	122.9	122.3	0.9	5.665	107.6	105.4
	1.0	1.947	116.0	120.0	1.1	4.616	114.3	112.1	1.2	7.705	96.74	93.85
	1.5	2.634	122.9	122.9	1.5	6.478	104.5	100.5	1.5	9.801	87.12	83.87
4^+	0.7	3.832	4.202	2.162	0.9	6.633	15.51	13.92	1.1	9.663	68.63	71.57
	1.1	5.974	11.40	9.314	1.2	8.556	42.12	43.06	1.3	10.97	94.46	99.35
	1.5	7.963	30.76	30.82	1.5	10.10	75.09	82.34	1.5	12.34	110.2	115.4

$\alpha+\alpha$ (without Coulomb) THSR framework

	2nd eigenstate				3rd eigenstate				4th eigenstate			
0^+	0.5	1.362	69.68	69.90	0.7	3.720	16.72	17.66	0.9	6.979	−22.88	−21.22
	1.0	3.194	27.43	26.44	1.1	6.214	−13.38	−13.74	1.2	9.568	−42.56	−42.50
	1.5	5.306	−3.370	−3.786	1.5	8.889	−38.31	−37.39	1.5	12.27	−61.27	−60.38
	1st eigenstate				2nd eigenstate				3rd eigenstate			
2^+	0.5	1.347	77.60	85.37	0.7	2.871	122.2	122.2	0.9	5.676	106.5	105.3
	1.0	1.973	115.0	120.4	1.1	4.627	113.6	112.0	1.2	7.717	95.89	93.76
	1.5	2.678	121.9	122.8	1.5	6.496	103.5	100.4	1.5	9.819	86.05	83.84
4^+	0.8	4.377	4.657	3.292	1.0	7.317	21.80	21.01	1.1	9.678	67.54	72.02
	1.2	6.492	14.76	12.78	1.3	9.109	53.74	56.98	1.3	10.97	94.44	99.31
	1.5	7.963	30.76	30.83	1.5	10.10	75.08	82.37	1.5	12.34	110.2	115.4

those from the R-matrix method also enlarges. This deviation becomes particularly pronounced, especially for lower energy levels.

As an example of the final computed results, we also present in Table I the phase shifts obtained by MCM-HOT and R-matrix method with some typical values of ω for the first few eigenvalues. In the R-matrix method, the parameters utilized for RGM, GCM, and THSR computations are also listed therein.

IV. CONCLUSIONS

In this work, we have provided a generalized framework named microscopic cluster model in harmonic oscillator trap (MCM-HOT) to extract the scattering phase shifts. This new approach can be adapted to various microscopic cluster methods such as RGM, GCM, THSR wave function method, and so on.

As a validation example, we have calculated the elastic scattering phase shifts for $\frac{1}{2}^+$, $\frac{1}{2}^-$, and $\frac{3}{2}^-$ states of

$\alpha + n$ system within the RGM framework. The results of MCM-HOT exhibit good agreement with those obtained through the traditional microscopic R-matrix method. Additionally, we have studied the $\alpha + \alpha$ system (without Coulomb interaction) within the GCM and THSR frameworks. The numerical results obtained by MCM-HOT also confirms its reliability. For more complicated clusters and heavier nuclei, the techniques of GCM is more concise compared to RGM in practice, therefore the further development and extension of MCM-HOT within GCM may be more systematical and powerful to compute the scattering phase shift. Additionally, in the numerical solutions of bound states, we introduce the complex virial theorem in the microscopic cluster model to ensure that the discrete energy spectra are sufficiently accurate not to impact on the application of the BERW formula. The complex virial theorem also encompasses the case of resonant states thus can be of assistance when dealing with the complex scaled cluster model.

In summary, we propose a new approach MCM-HOT and employ it to conduct a preliminary investigation of elastic scattering phase shifts in single-channel two-cluster systems without Coulomb interaction. Incorporating the Coulomb interaction in the trap method is relatively complicated to handle [49] and we will conduct a detailed discussion and study on systems involving the Coulomb potential in our future work.

ACKNOWLEDGMENTS

This work is supported by the National Natural Science Foundation of China (Grants No. 11975167, No. 12035011, No. 11905103, No. 11947211, No. 11761161001, No. 11961141003, and No. 12022517), by the National Key R&D Program of China (Contracts No. 2018YFA0404403, No. 2016YFE0129300, and No. 2023YFA1606503), by the Science and Technology Development Fund of Macau (Grants No. 0048/2020/A1 and No. 008/2017/AFJ), by the Fundamental Research Funds for the Central Universities (Grants No. 22120210138 and No. 22120200101).

APPENDIX A: COMPLEX VIRIAL THEOREM IN MICROSCOPIC CLUSTER MODEL

With the help of complex scaling method, the original virial theorem can be extended to the complex energy plane [50]. Therefore, we refer to it as the complex virial theorem in the following. In microscopic cluster model, we still base on the variational principle and obtain the complex virial theorem in MCM:

$$\frac{\partial}{\partial\eta}\frac{(\phi|H(\eta)|\phi)}{(\phi|N(\eta)|\phi)} = 0\ (\eta = e^{i\theta}) \rightarrow \begin{cases} \dfrac{\partial_\eta(\phi|H(\eta r,\eta r')|\phi)}{\partial_\eta(\phi|(1-\eta N(\eta r,\eta r'))|\phi)} = \dfrac{(\phi|H(\eta r,\eta r')|\phi))}{(\phi|(1-\eta N(\eta r,\eta r'))|\phi)} = E_{\text{exact}}, & \text{for RGM} \\ \dfrac{\partial_\eta(\phi(b\eta^{-1})|H(\eta r)|\phi(b\eta^{-1}))}{\partial_\eta(\phi(b\eta^{-1})|\phi(b\eta^{-1}))} = \dfrac{(\phi(b\eta^{-1})|H(\eta r)|\phi(b\eta^{-1}))}{(\phi(b\eta^{-1})|\phi(b\eta^{-1}))} = E_{\text{exact}}, & \text{for GCM and THSR} \end{cases}, \tag{A1}$$

where $N(r, r')$ is the exchange norm kernel in RGM, b is the oscillator parameter. These formulas hold at the exact wave function ϕ and E_{exact} is the exact eigenenergy (bound state or resonance) of the Schrödinger equation. The parentheses "()" used above denote the c product required by the non-Hermitian nature, which is induced by the complex scaling transformation. The complex virial theorem for GCM and TSHR mentioned above can be easily derived from the complex scaled cluster model [23,51]. The energy spectrum of the trapped system is composed of discrete bound states, therefore we can simply set the complex scaling angle θ to 0 in MCM-HOT. However, for the sake of generality, we still provide the form that includes η below.

Explicitly speaking, we have the following expressions in the framework of RGM, GCM and THSR, respectively:

RGM framework.

complex scaled Hamiltonian: $H(\eta r, \eta r') = \eta^{-2}T + V(\eta r) + \eta W(\eta r, \eta r')$

$$\begin{aligned}\frac{2}{\eta^2}(\phi|T|\phi) = &\left(\phi|\eta r\frac{\partial V(\eta r)}{\partial \eta r}|\phi\right) + \left(\phi|\eta W(\eta r,\eta r') + \eta^2 r\frac{\partial W(\eta r,\eta r')}{\partial \eta r} + \eta^2 r'\frac{\partial W(\eta r,\eta r')}{\partial \eta r'}|\phi\right) \\ &+ E_{exact}\left(\phi|\eta N(\eta r,\eta r') + \eta^2 r\frac{\partial N(\eta r,\eta r')}{\partial \eta r} + \eta^2 r'\frac{\partial N(\eta r,\eta r')}{\partial \eta r'}|\phi\right),\end{aligned} \tag{A2}$$

where $V(r)$ and $W(r, r')$ represent the local and nonlocal potential, respectively. This formula can be regarded as an extension of the original virial theorem to nonlocal interactions.

GCM framework.

Assuming the exact wave function ϕ can be approximately expressed as a superposition of a finite set of basis functions $\psi(R)$ (R represents the generator coordinate): $\phi = \sum_i C_i\psi(R_i)$. Therefore the complex virial theorem for GCM can be expressed as

$$\begin{aligned}\frac{\partial_\eta\left(\sum_i C_i\psi(\eta R_i)|H|\sum_j C_j\psi(\eta R_j)\right)}{\partial_\eta\left(\sum_i C_i\psi(\eta R_i)|\sum_j C_j\psi(\eta R_j)\right)} &= \frac{\sum_{i,j} C_iC_j[R_i\partial_{\eta R_i}(\psi(\eta R_i)|H|\psi(\eta R_j)) + R_j\partial_{\eta R_j}(\psi(\eta R_i)|H|\psi(\eta R_j))]}{\sum_{i,j} C_iC_j[R_i\partial_{\eta R_i}(\psi(\eta R_i)|\psi(R_j)) + R_j\partial_{\eta R_j}(\psi(\eta R_i)|\psi(R_j))]} \\ &= \frac{\left(\sum_i C_i\psi(\eta R_i)|H|\sum_j C_j\psi(\eta R_j)\right)}{\left(\sum_i C_i\psi(\eta R_i)|\sum_j C_j\psi(\eta R_j)\right)} = E_{\text{exact}}.\end{aligned} \tag{A3}$$

THSR framework.

Similar to the case of GCM, we only need to replace the generator coordinate R with the deformation parameter $\boldsymbol{\beta} = (\beta_x, \beta_y, \beta_z)$:

$$\frac{\partial_\eta\left(\sum_i C_i\psi(\eta\boldsymbol{\beta}_i)|H|\sum_j C_j\psi(\eta\boldsymbol{\beta}_j)\right)}{\partial_\eta\left(\sum_i C_i\psi(\eta\boldsymbol{\beta}_i)|\sum_j C_j\psi(\eta\boldsymbol{\beta}_j)\right)} = \frac{\sum_{i,j} C_iC_j[\boldsymbol{\beta}_i\nabla_{\eta\boldsymbol{\beta}_i}(\psi(\eta\boldsymbol{\beta}_i)|H|\psi(\eta\boldsymbol{\beta}_j)) + \boldsymbol{\beta}_j\nabla_{\eta\boldsymbol{\beta}_j}(\psi(\eta\boldsymbol{\beta}_i)|H|\psi(\eta\boldsymbol{\beta}_j))]}{\sum_{i,j} C_iC_j[\boldsymbol{\beta}_i\nabla_{\eta\boldsymbol{\beta}_i}(\psi(\eta\boldsymbol{\beta}_i)|\psi(\boldsymbol{\beta}_j)) + \boldsymbol{\beta}_j\nabla_{\eta\boldsymbol{\beta}_j}(\psi(\eta\boldsymbol{\beta}_i)|\psi(\boldsymbol{\beta}_j))]}$$
$$= \frac{\left(\sum_i C_i\psi(\eta\boldsymbol{\beta}_i)|H|\sum_j C_j\psi(\eta\boldsymbol{\beta}_j)\right)}{\left(\sum_i C_i\psi(\eta\boldsymbol{\beta}_i)|\sum_j C_j\psi(\eta\boldsymbol{\beta}_j)\right)} = E_{\text{exact}}. \tag{A4}$$

For GCM and THSR frameworks, if the Hamiltonian and norm kernels can be obtained analytically, the kernels involving derivative can also conveniently derived in the analytical forms.

APPENDIX B: HARMONIC OSCILLATOR TRAP IN GCM AND THSR FRAMEWORKS

We take the α-α system without Coulomb potential as an example to illustrate the application of the MCM-HOT within both GCM and THSR frameworks. For this system, we use all the same parameters as the original ones in Ref. [51], namely, $b = 1.36$ fm, Majorana exchange parameter $M = 0.573$, and Volkov No. 1 force adopted as the effective two-body nuclear interaction. Besides, in THSR wave function method we only handle the case of axially symmetric deformation with the z axis being the symmetry axis, namely, $\beta_x = \beta_y = \beta_\perp \neq \beta_z$.

The kernels of the harmonic oscillator potential can be introduced through the asymptotic relative waves function as follows:

$$V_{H.O.}(R, R') = \langle\Gamma_L(R, r)|\,\tfrac{1}{2}\mu\omega^2 r^2\,|\Gamma_L(R', r)\rangle\,,\ \text{for GCM}$$
$$V_{H.O.}(\boldsymbol{\beta}, \boldsymbol{\beta}') = \langle\Gamma_L(\boldsymbol{\beta}, r)|\,\tfrac{1}{2}\mu\omega^2 r^2\,|\Gamma_L(\boldsymbol{\beta}', r)\rangle\,,\ \text{for THSR}, \tag{B1}$$

where Γ_L denotes the asymptotic relative wave function with angular momentum L:

$$\Gamma_L(R, r) = \left(\frac{2}{\pi b^2}\right)^{\frac{3}{4}} e^{-\frac{(r^2+R^2)}{b^2}} i_L\left(\frac{2rR}{b^2}\right),\ \text{for GCM}$$
$$\Gamma_L(\beta_\perp, \beta_z, r) = (2\pi)^{3/2}\beta_x\beta_y\beta_z\left(\frac{2}{\pi}\right)^{3/4}\frac{b^{3/2}}{(b^2+2\beta_\perp^2)(b^2+2\beta_z^2)^{1/2}}\exp\left(-\frac{r^2}{b^2+2\beta_\perp^2}\right)$$
$$\times\int d\cos(\theta)P_L(\cos(\theta))\exp(-r^2\cos^2(\theta)\frac{2\left(\beta_\perp^2-\beta_z^2\right)}{(b^2+2\beta_\perp^2)\left(b^2+2\beta_z^2\right)}),\ \text{for THSR}, \tag{B2}$$

where θ is the angle between $\boldsymbol{r}$ and z axis, i_L is the modified spherical Bessel function of the first kind, $P_L(x)$ is the Legendre function. Details of the derivation can be found in Ref. [24].

[1] J. A. Wheeler, Phys. Rev. **52**, 1107 (1937).
[2] J. A. Wheeler, Phys. Rev. **52**, 1083 (1937).
[3] D. Thompson, M. Lemere, and Y. Tang, Nucl. Phys. A **286**, 53 (1977).
[4] K. Wildermuth, Y. C. Tang, and E. Sheldon, Phys. Today **30**, 62 (1977).
[5] Y. C. Tang, in *Topics in Nuclear Physics II A Comprehensive Review of Recent Developments*, edited by T. T. S. Kuo and S. S. M. Wong (Springer, Berlin/Heidelberg, 1981), pp. 571–692.
[6] H. Horiuchi, Prog. Theor. Phys. **43**, 375 (1970).
[7] H. Horiuchi, Prog. Theor. Phys. Suppl. **62**, 90 (1977).
[8] H. Horiuchi and K. Ikeda, in *Cluster Models and Other Topics*, edited by Y. Akaishi *et al.* (World Scientific Publishing Co. Pte. Ltd, Singapore, 1986), pp. 1–258.
[9] A. Tohsaki, H. Horiuchi, P. Schuck, and G. Röpke, Phys. Rev. Lett. **87**, 192501 (2001).
[10] B. Zhou, Y. Funaki, H. Horiuchi, Z. Ren, G. Röpke, P. Schuck, A. Tohsaki, C. Xu, and T. Yamada, Phys. Rev. Lett. **110**, 262501 (2013).
[11] A. Tohsaki, H. Horiuchi, P. Schuck, and G. Röpke, Rev. Mod. Phys. **89**, 011002 (2017).
[12] T. Myo, Y. Kikuchi, H. Masui, and K. Katō, Prog. Part. Nucl. Phys. **79**, 1 (2014).
[13] M. Odsuren, K. Katō, M. Aikawa, and T. Myo, Phys. Rev. C **89**, 034322 (2014).
[14] S. Aoyama, T. Myo, K. Katō, and K. Ikeda, Prog. Theor. Phys. **116**, 1 (2006).
[15] T. Berggren, Nucl. Phys. A **109**, 265 (1968).
[16] N. Michel, W. Nazarewicz, M. Płoszajczak, and T. Vertse, J. Phys. G: Nucl. Part. Phys. **36**, 013101 (2009).
[17] D. Baye, P.-H. Heenen, and M. Libert-Heinemann, Nucl. Phys. A **291**, 230 (1977).
[18] P. Descouvemont and D. Baye, Rep. Prog. Phys. **73**, 036301 (2010).
[19] D. Bai and Z. Ren, Phys. Rev. C **101**, 034311 (2020).
[20] D. Bai and Z. Ren, Phys. Rev. C **103**, 014612 (2021).
[21] K. Arai and A. T. Kruppa, Phys. Rev. C **60**, 064315 (1999).
[22] R. Suzuki, A. T. Kruppa, B. G. Giraud, and K. Katō, Prog. Theor. Phys. **119**, 949 (2008).

[23] T. Myo and H. Takemoto, Phys. Rev. C **107**, 064308 (2023).
[24] H. Zhang, D. Bai, Z. Wang, and Z. Ren, Phys. Rev. C **107**, 064304 (2023).
[25] T. Busch, B.-G. Englert, K. Rzazewski, and M. Wilkens, Found. Phys. **28**, 549 (1998).
[26] X. Zhang, Phys. Rev. C **101**, 051602(R) (2020).
[27] T. Luu, M. J. Savage, A. Schwenk, and J. P. Vary, Phys. Rev. C **82**, 034003 (2010).
[28] X. Zhang, S. R. Stroberg, P. Navrátil, C. Gwak, J. A. Melendez, R. J. Furnstahl, and J. D. Holt, Phys. Rev. Lett. **125**, 112503 (2020).
[29] M. Bagnarol, M. Schäfer, B. Bazak, and N. Barnea, Phys. Lett. B **844**, 138078 (2023).
[30] I. Stetcu, J. Rotureau, B. Barrett, and U. van Kolck, Ann. Phys. **325**, 1644 (2010).
[31] C.-J. Yang, Phys. Rev. C **94**, 064004 (2016).
[32] P. Guo and B. Long, J. Phys. G: Nucl. Part. Phys. **49**, 055104 (2022).
[33] J. Rotureau, I. Stetcu, B. R. Barrett, and U. van Kolck, Phys. Rev. C **85**, 034003 (2012).
[34] J. Rotureau, I. Stetcu, B. R. Barrett, M. C. Birse, and U. van Kolck, Phys. Rev. A **82**, 032711 (2010).
[35] I. Stetcu, B. R. Barrett, U. van Kolck, and J. P. Vary, Phys. Rev. A **76**, 063613 (2007).
[36] P. Descouvemont and M. Dufour, Microscopic cluster models, in *Clusters in Nuclei*, edited by C. Beck (Springer, Berlin/Heidelberg, 2012), Vol. 2, pp. 1–66.
[37] T. Yamada, Y. Funaki, H. Horiuchi, G. Röpke, P. Schuck, and A. Tohsaki, Nuclear alpha-particle condensates, in [36], pp. 229–298.
[38] S. Blinder, J. Math. Phys. **25**, 905 (1984).
[39] DLMF, NIST Digital Library of Mathematical Functions, release 1.1.11 of 2023-09-15, edited by f. W. J. Olver, A. B. Olde Daalhuis, D. W. Lozier, B. I. Schneider, R. F. Boisvert, C. W. Clark, B. R. Miller, B. V. Saunders, H. S. Cohl, and M. A. McClain, https://dlmf.nist.gov/.
[40] B. Borasoy, E. Epelbaum, H. Krebs, D. Lee, and U.-G. Meissner, Eur. Phys. J. A **34**, 185 (2007).
[41] A. Rokash, M. Pine, S. Elhatisari, D. Lee, E. Epelbaum, and H. Krebs, Phys. Rev. C **92**, 054612 (2015).
[42] S. Elhatisari, D. Lee, U.-G. Meissner, and G. Rupak, Eur. Phys. J. A **52**, 174 (2016).
[43] P. Guo and V. Gasparian, Phys. Rev. D **103**, 094520 (2021).
[44] Y. Suzuki, D. Baye, and A. Kievsky, Nucl. Phys. A **838**, 20 (2010).
[45] D. R. Thompson, I. Reichstein, W. McClure, and Y. C. Tang, Phys. Rev. **185**, 1351 (1969).
[46] I. Reichstein and Y. C. Tang, Nucl. Phys. A **158**, 529 (1970).
[47] M. Theeten, D. Baye, and P. Descouvemont, Phys. Rev. C **74**, 044304 (2006).
[48] M. Hesse, J. Roland, and D. Baye, Nucl. Phys. A **709**, 184 (2002).
[49] H. Zhang, D. Bai, Z. Wang, and Z. Ren, Phys. Lett. B **850**, 138490 (2024).
[50] E. Brändas and P. Froelich, Phys. Rev. A **16**, 2207 (1977).
[51] H. Zhang, D. Bai, Z. Wang, and Z. Ren, Phys. Rev. C **105**, 054317 (2022).